This is the peer-reviewed, final accepted version for American Mineralogist, published by the Mineralogical Society of America.
The published version is subject to change. Cite as Authors (Year) Title. American Mineralogist, in press.
DOI: https://doi.org/10.2138/am-2020-7405. http://www.minsocam.org/

REVISION 1:

Formation of metasomatic tourmalinites in reduced schists during the Black Hills Orogeny, South Dakota

PETER I. NABELEK

Department of Geological Sciences, University of Missouri, Columbia, Missouri 65211, U.S.A.

E-mail: nabelekp@missouri.edu

This is the peer-reviewed, final accepted version for American Mineralogist, published by the Mineralogical Society of America.
The published version is subject to change. Cite as Authors (Year) Title. American Mineralogist, in press.
DOI: https://doi.org/10.2138/am-2020-7405. http://www.minsocam.org/

ABSTRACT

Tourmaline is a common mineral in granites and metamorphic rocks in collisional orogens. This paper describes graphite-bearing, metasomatic tourmalinites in sillimanite-zone schists of the Proterozoic Black Hills Orogen, South Dakota. The tourmalinites bound quartz veins and beyond about 1 m grade into schists with disseminated tourmaline, and ultimately tourmaline becomes only a trace, intrinsic phase in the schists. Next to the quartz veins tourmaline has almost completely replaced schist minerals, including biotite, muscovite, and plagioclase. The tourmaline is generally anhedral and follows the original foliation direction of the schist. However, tourmaline is euhedral in quartz veinlets cutting through the tourmalinites. Tourmaline is compositionally zoned from having about 22% to 2% of apparent Al occupancy on the Y sites. There are very good negative correlations of $^{Y}(Fe^{2+}+Mg^{2+})$, $^{X}Ca^{2+}$, and $^{Y}Ti^{4+}$ with $^{Y}Al^{3+}$, and a very good positive correlation of X-site vacancies with $^{Y}Al^{3+}$. Mg# [molar $Mg^{2+}/(Mg^{2+}+Fe^{2+})$] is fairly invariant at approximately 0.5, which is somewhat higher than that in the precursor biotite. This is in contrast to tourmaline in the neighboring peraluminous Harney Peak leucogranite where the range of Y site occupancy of Al is small at about 20%, but the Mg# ranges from 0.12 to 0.5.

The compositional trends in the metasomatic tourmaline are dominated by the exchange $^{X}\square + 4\ ^{Y}Al^{3+} = {}^{X}Ca^{2+} + 3\ ^{Y}(Fe^{2+}+Mg^{2+}) + {}^{Y}Ti^{4+}$. Mass-balance calculations suggest the metasomatizing fluid brought in H^{+} and $B(OH)_3$ and removed K^{+}, SiO_2, and some Fe^{2+} during tourmalinization. Other elements in the tourmaline largely reflect the bulk composition of the replaced schist. The calculations show that silica in the quartz veins was locally derived, not brought in by the metasomatizing fluid. Interstitial graphite in the tourmalinites shows

precipitation of carbon from the methane-bearing fluid. The study demonstrates an important effect of boron transfer by fluids during metamorphism and magmatism in the Earth's crust.

Keywords: Tourmaline, tourmalinite, metasomatism, schist, fluid, Black Hills

INTRODUCTION

Relatively high abundances of boron and its common mineral host, tourmaline, are frequent features of collisional granites and metapelites (Henry and Guidotti 1985; Nabelek et al. 1992a; Guillot and Le Fort 1995; Nabelek and Bartlett 1998; Nabelek 2019). High abundances of B in metapelites stem from its incorporation into ocean floor sediments (Leeman and Sisson 1996). Boron may be conserved in metapelites during prograde metamorphism if it is contained by tourmaline (Henry and Dutrow 1996; Wilke et al. 2002), but if instead bulk of it resides in micas, some of it may be lost from rocks by aqueous fluids produced by mica-consuming metamorphic reactions (Nabelek et al. 1990; Moran et al. 1992; Leeman and Sisson 1996). Ultimately, when all muscovite is consumed from schists during partial melting, most B is incorporated into the melts, although a portion may be retained in residual sillimanite (Grew and Hinthorne 1983). An important feature of B is that it is highly mobile in aqueous fluids as is evident by experiments (Pichavant 1981), frequent association of tourmaline with veins of hydrothermal origin, either as a replacement mineral or a primary mineral (Slack 1996), and by frequent enrichments of B in aureoles of granitic pegmatites, either within micas or in newly-formed tourmaline (Shearer et al. 1984; Shearer et al. 1986; Duke 1995; Wilke et al. 2002).

This contribution describes a tourmalinite next to a quartz vein in a sillimanite-grade schist in the aureole of the Harney Peak Granite (HPG) in the Black Hills, South Dakota, USA (Figs. 1, 2). The granite, associated pegmatites, schists, and metagraywackes occur within the

Proterozoic core of the Black Hills. The core is a classic orogenic sedimentary wedge that became deformed and metamorphosed during the Proterozoic Black Hills orogeny that was a consequence of the collision of the Archean Wyoming and Superior cratonic blocks. Tourmaline characterizes large portions of the HPG and some pegmatites and is a common metasomatic phase in the metamorphic aureoles that affect the surrounding metapelitic rocks. Although Slack (1996) defined tourmalinite as a metasomatized rock with more than 15% tourmaline, at the locality described here metasomatism was unusually intense with tourmaline effectively completely replacing a quartz-mica schist. Such tourmalinites also occur at other localities in the western aureole of the HPG. The tourmalinites include interstitial graphite and occur next to quartz veins.

The focus of this contribution is on the crystal-chemistry of tourmaline as a recorder of the tourmalinization process and composition of the metasomatizing fluid. Compositions of tourmaline and micas reveal the solutes that were in the metasomatizing fluid and the ion-exchange reactions that were responsible for the tourmalinization reactions. Such fluids are likely to exist in deep orogenic wedges undergoing metamorphism during continental collisions, and therefore are an important part of the crustal boron cycle.

GEOLOGIC BACKGROUND

Metamorphism and magmatism in the Black Hills were previously described in several papers (e.g., Norton and Redden 1990; Helms and Labotka 1991; Nabelek et al. 1992a, b, 2006; Nabelek and Chen 2014). The Proterozoic core of the Black Hills was exposed by late-Mesozoic to early-Tertiary Laramide uplift and erosion (Redden et al. 1990). Protoliths of the metamorphic rocks were shales with variable amounts of organic components, graywackes, mafic sills, and to

the southeast of the HPG a sandstone (Fig. 1). Metamorphism occurred during a polyphase deformational history. Evidence for the earliest metamorphism (M_1) and deformation (D_1) appears to be restricted to the western margin of the terrane. They were attributed to a regional thrusting related to Yavapai arc accretion from the south between 1790 and 1750 Ma (Dahl et al. 1999, 2005). However, metamorphism (M_2) and deformation (D_2) that dominate the structure of the Proterozoic terrane are related to east-west shortening during the Black Hills Orogeny beginning at c. 1750 Ma (Redden et al. 1990; Chamberlain et al. 2003; Dahl et al. 2005).

Late-orogenic intrusion of the HPG in the southern Black Hills superimposed contact metamorphism (M_3) and associated deformation (D_3) on the regionally metamorphosed rocks. Intrusion of the granite occurred at c. 1715 Ma (Redden et al. 1990). The HPG pluton and a large pegmatite field are the dominant geologic features of the southern Black Hills (Norton and Redden, 1990). The HPG was built-up by intrusion of many thousands of leucogranite sills and dikes. Most pegmatite intrusions occur in schists and metagraywackes. In close proximity to the HPG, the intrusion of magma transposed the regional S_2 foliation in metamorphic rocks into S_3, which is more horizontal and generally concordant with granite sills that constructed the HPG (Duke et al. 1988, 1990b). The M_2 and M_3 metamorphic events probably overlapped in time (Redden and DeWitt 2008). Maximum metamorphic pressures in the aureole of the HPG were at least 6 kbar but the aureole appears to have decompressed to about 3 kbar as the granite was being emplaced, probably due to buoyancy (Nabelek and Chen 2014).

Fluids were present in the metamorphic rocks during the M_2 and M_3 metamorphic events. Compositions of fluid inclusions in quartz veins show that reducing conditions prevailed (Huff and Nabelek, 2007). During M_2, the fluids were dominated by variable proportions of CH_4, CO_2 and N_2. Application of the Andersen and Lindsley (1988) oxygen barometer to Mn-bearing

ilmenite and magnetite-ulvöspinel pairs in some garnet-grade samples suggests that fO_2 was 4.6 ± 1.1 log units below the fayalite-magnetite-quartz oxygen buffer. Graphite in the schists ranges from poorly ordered in the garnet zone to well-ordered within the sillimanite zone in the HPG contact aureole (Huff and Nabelek 2007). Fluids in the aureole of the HPG had ~25% of carbonic components. Well-ordered graphite commonly occurs along margins of quartz veins and host rocks to the veins (Duke et al. 1990a). In the samples described here, graphite is highly ordered with area ratios of "disordered/ordered" Raman peaks between 0 and 0.1, and fluid inclusions in the quartz vein have >90% CH_4 (Huff and Nabelek 2007).

A large portion of fluids in the HPG aureole and aureoles of pegmatite intrusions was magmatic. The fluids caused alkali (Na, K, Li) and B metasomatism of schists and graywackes on various scales (Duke 1995; Wilke et al. 2002; Nabelek et al. 2006; Teng et al. 2006). Fluid flow was probably preferentially concentrated on and near faults that bound the HPG as most intense metasomatism appears to have occurred there. Moreover, tourmalinites described here come from a locality that may have beneath it a portion of the Harney Peak Granite (Duke et al., 1990b), from which the metasomatizing fluid may have emanated.

The HPG in its outer portions contains abundant tourmaline. The inner portions tend to have biotite instead of tourmaline as the dominant ferromagnesian mineral. Tourmaline ranges from the millimeter scale in aplitic granite layers, in which it may define color banding (often called "line rock"), to the decimeter scale in pegmatitic layers (Rockhold et al., 1987, Duke et al., 1988). In pegmatite sheets, both within the granite and the wall rocks, it is oriented almost invariably with the long *c*-axis perpendicularly to the contacts between the sheets and intruded rocks. Tourmaline's orientation within the intrusive sheets follows the probable direction of heat loss from the crystallizing sheets.

ANALYTICAL TECHNIQUE AND DATA REDUCTION

Tourmaline, biotite, and muscovite in tourmalinites were analyzed for major elements by a JEOL JXA-8200 electron microprobe at Washington University, St. Louis, Missouri. The operating conditions were 15 keV accelerating voltage, 25 nA specimen current, 5-10 μm beam diameter, and 11 mm working distance. The Mean Atomic Number correction method of Donovan et al. (2016) was used to calculate wt.% of oxides in the minerals. For tourmaline, Si, Ti, Al, Fe, Mn, Mg, Zn, Ca, Na, and K were sought, but Zn was below the detection limit and K_2O was always <0.02 wt.%. F was analyzed in only a subset of tourmaline.

Atomic site assignments in tourmaline, given its formula $XY_3Z_6(T_6O_{18})(BO_3)_3V_3W$, followed the scheme recommended by Henry et al. (2011). Thirty-one oxygens per formula unit were assumed. The weight percents of H_2O and B_2O_3 were iteratively adjusted to obtain 3 B atoms and 15 other cations in Y+Z+T sites. Vacancies can exist on the X sites. The V and W sites are filled by either OH^-, F^-, or O^{2-}, but here for simplicity, it is assumed that F^- and O^{2-} occur only on the W sites. Given the reducing conditions of the environment in which the tourmalinites formed, all Fe was assumed to be ferric. Compositions of tourmaline with minimum and maximum amounts of apparent $^{Y}Al^{3+}$ in each sample are given in Table 1. Site assignments for biotite and muscovite were calculated by assuming 12 O^{2-} anions and two H^+ cations. All mineral analyses are given in Supplementary Material.

PETROGRAPHY OF TOURMALINITE

Tourmalinites described here replaced schists and occur next to quartz veins. This style of occurrence differs from tourmalinites that occur as breccia tourmaline-quartz veins at relatively

low-pressure localities (e.g., Dini et al. 2008) or gold-bearing tourmaline-quartz veins (e.g., Olivo and Williams-Jones 2002). Samples 195-1, 195-3A, B, and 195-5 represent the metasomatic progression from nearly wholly replaced schist to one with only disseminated tourmaline. Sample 195-3A is a 7 mm thick quartz-tourmaline vein that cuts through sample 195-3B. In samples 195-1 and 195-3B, interstices between tourmaline grains are mostly filled with graphite (Fig. 3a, c). There are occasional interstitial quartz grains, but most quartz occurs as rounded, anhedral inclusions within tourmaline. Tourmaline within 195-3A is euhedral (Fig. 3b). A few grains of pyrrhotite occur in 195-3B. Foliated muscovite, biotite, and quartz dominate sample 195-5, and graphite is much less abundant in it than in the other samples. Plagioclase and minor ilmenite also occur in the sample. Tourmaline is generally euhedral (Fig. 3d).

Petrography of samples 195-1 and 195-3B shows apparent alignment of tourmaline grains that corresponds with the local foliation direction in unmetasomatized schist (Fig. 3c). It is unclear whether the tourmaline foliation is due to compression of the tourmaline itself, or whether the tourmaline merely mimics the foliation direction of replaced micas. Tourmaline within 195-3A (quartz vein) and 195-5 appears to be randomly oriented (Fig. 3b, d). The random orientation of tourmaline in sample 195-5 suggests that the bulk of its crystals grew after the development of foliation. Because intrusion of the HPG and pegmatites was the last major event of the Black Hills Orogeny, and some minerals, particularly staurolite, in the aureole of the HPG overgrew the D_3 foliation, the metasomatism at location 195 appears to have been related to the late-orogenic magmatism in the region.

Zoning of tourmaline in sample 195-5 is not apparent by either petrography and back-scatter electron (BSE) imaging. On the other hand, zoning of tourmaline is revealed by both techniques in samples 195-1, 195-3A, and 195-3B. In BSE images, most tourmaline grains in

195-1 and 195-3 have fairly bright, broad cores that trend outward toward even brighter zones (Fig. 4a). The shapes of the brighter zones are not well defined. The rims of the grains are gray. In sample 195-3A, the zoning is more pronounced and the shape of zoning is consistent with the euhedral crystal shapes. The cores are gray but become brighter outward. The rims of the grains are again gray. The brightness of the zones correlates mostly with Fe concentration. There is no obvious evidence for detrital grains in any of the tourmaline images. Petrographically in plain light, the most intense zoning of tourmaline appears in 195-3A where it ranges from green in cores to brown outward toward rims (Fig. 3b). However, the very rims have less intense brown color.

COMPOSITIONAL ZONING IN TOURMALINE

Chemical variations in the metasomatic tourmaline are best considered in view of the formula $XY_3Z_6(T_6O_{18})(BO_3)_3V_3W$. In the stoichiometric schorl end-member, the X site is filled with Na^+, the Y sites are filled with Fe^{2+}, the Z sites are filled with Al^{3+}, the T sites are filled with Si^{4+}, the V sites are filled with OH^- or O^{2-}, and the W site is filled with OH^-, O^{2-}, or F^- (Henry et al. 2011). In the dravite end-member, the Y sites are filled with Mg^{2+} instead of Fe^{2+}. When Al^{3+} partially occupies the Y sites, it is frequently assumed that its charge is balanced by Li^+ also in the Y sites, which makes up the elbaite component. Although Li was not measured in the metasomatic tourmaline, analysis of schorl-dravite tourmaline in high-Li pegmatites shows that Li concentrations are only up to ~1000 ppm by weight (Maloney et al. 2008). Published data suggests that there is only a limited solubility of the elbaite component in dravite-bearing tourmaline, such that there appears to exist a complete solution only between dravite-poor

200 tourmaline and elbaite (Henry and Guidotti 1985; Jolliff et al. 1986; Henry and Dutrow 1992,
201 1996; Keller et al. 1999).

202 The metasomatic tourmaline in the Black Hills has sub-equal proportions of schorl and
203 dravite components with up to 22% Al^{3+} in the Y site (Fig 5a). The highest Mg^{2+}/Fe^{2+} is in
204 tourmaline 195-5, probably due to the preferential partitioning of Mg over Fe into tourmaline
205 relative to biotite (Henry and Guidotti, 1985). The Mg^{2+}/Fe^{2+} ratios in the metasomatic
206 tourmaline are on the high end of the tourmaline composition trend in the HPG (Fig. 5a), but the
207 HPG tourmaline (Supplementary Material) does not trend toward zero $^{Y}Al^{3+}$. There is no
208 correlation of Mg^{2+}/Fe^{2+} with $^{Y}Al^{3+}$ in the metasomatic tourmaline. The Mg# of all metasomatic
209 tourmaline is higher than that of biotite in sample 195-5 and in most analyzed metapelites in the
210 Black Hills (Fig. 5b). The correspondence of major element biotite compositions in 195-5 with
211 compositions of biotite in other metapelites shows that its composition was not affected by
212 metasomatism to any significant extent.

213 The metasomatic tourmaline shows remarkably good negative correlations of $^{Y}(Fe^{2+}+$
214 $Mg^{2+})$, $^{X}Ca^{2+}$, and $^{Y}Ti^{4+}$ with $^{Y}Al^{3+}$ (Fig. 6a, b; Table 2). There is also a very good positive
correlation of X-site vacamM^{2+}

313

314 ## IMPLICATIONS

315 The tourmalinites described here and abundant metasomatic tourmaline in the aureoles of
316 the Harney Peak Granite and pegmatites in the Black Hills (Shearer et al. 1984, 1986; Duke
317 1995) demonstrate a high mobility of boron through metamorphic rocks in collisional orogens. In
318 the case presented here, the activity of boron in the fluid was sufficiently high to cause an
319 effectively complete replacement of muscovite, biotite, quartz, and feldspar in schists. Because
320 oceanic sediments that are protoliths to orogenic schists commonly contain organic components,
321 the metamorphic environment was highly reducing. Thus, methane is likely to accompany boron
322 in the fluid and ultimately cause precipitation of graphite along with tourmaline. In a way,
323 tourmalinites in collisional orogens are reflections of the end of a boron cycle that beings with
324 absorption of boron from seawater into clays on the ocean floor, continues with its incorporation
325 into partial melts that mark the limit of metamorphism of oceanic sediments, and ends with
326 expulsion of boron from the crystallizing melts back into the metamorphic aureoles of plutons.

327

328 ## ACKNOWLEDGEMENTS

329 Funding for this work was provided by NSF grant EAR-1321519. Paul Carpenter aided
330 with electron microprobe analysis at Washington University, St. Louis. The paper was improved
331 by constructive reviews of Derrell Henry and Shan Ke.

332

333

334

335

REFERENCES CITED

Andersen, D.J., and Lindsley, D.H. (1988) Internally consistent solution model for Fe-Mg-Mn-Ti oxides: Fe-Ti oxides. American Mineralogist, 73, 714-726.

Chamberlain, K.R., Frost, C.D., and Frost, B.R. (2003) Early Archean to Mesoproterozoic evolution of the Wyoming Province: Archean origins to modern lithospheric structure. Canadian Journal of Earth Sciences, 40, 1357-1374.

Dahl, P.S., Holm, D.K., Gardner, E.T., Hubacher, F.A., and Foland, K.A. (1999) New constraints on the timing of Early Proterozoic tectonism in the Black Hills (South Dakota), with implications for docking of the Wyoming province with Laurentia. Geological Society of America Bulletin, 111, 1335-1349.

Dahl, P.S., Terry, M.P., Jercinovic, M.J., Williams, M.L., Hamilton, M.A., Foland, K.A., Clement, S.M., and Friberg, L.M. (2005) Electron microprobe (Ultrachron) microchronometry of metamorphic monazite: Unraveling the timing of polyphase thermotectonism in the easternmost Wyoming craton (Black Hills, South Dakota). American Mineralogist, 90, 1712-1728.

Dini, A., Mazzarini, F., Musumeci, G., and Rocchi, S. (2008) Multiple hydro-fracturing by boron-rich fluids in the Late Miocene contact aureole of eastern Elba Island (Tuscany, Italy). Terra Nova, 20, 318-326.

Donovan, J.J., Singer, J.W., and Armstrong, J.T. (2016) A new EPMA method for fast trace element analysis in simple matrices. American Mineralogist, 101, 1839-1853.

Duke, E.F. (1995) Contrasting scales of element mobility in metamorphic rocks near Harney Peak Granite, Black Hills, South Dakota. Geological Society of America Bulletin, 107, 274-285.

359 Duke, E.F., Redden, J.A., and Papike, J.J. (1988) Calamity Peak layered granite-pegmatite
360 complex, Black Hills, South Dakota: Part I. Structure and emplacement. Bulletin of the
361 Geological Society of America, 100, 825-840.
362 Duke, E.F., Galbreath, K.C., and Trusty, K.J. (1990a) Fluid inclusion and carbon isotope studies
363 of quartz-graphite veins, Black Hills, South Dakota, and Ruby Range, Montana.
364 Geochimica et Cosmochimica Acta, 54, 683-698.
365 Duke, E.F., Shearer, C.K., Redden, J.A., and Papike, J.J. (1990b), Proterozoic granite-pegmatite
366 magmatism, Black Hills, South Dakota: Structure and geochemical zonation. In J.F.
367 Lewry and M.R. Stauffer, Eds., The Early Proterozoic Trans-Hudson Orogen, Geological
368 Association of Canada Special Paper, 37, 253-269.
369 Gallagher, V., and Kennan, P.S. (1992) Tourmaline on the margin of the Leinster Granite,
370 southeast Ireland: Petrogenetic implications. Irish Journal of Earth Sciences, 11, 131-150.
371 Grew, E.S., and Hinthorne, J.R. (1983) Boron in sillimanite, 221, 547-549.
372 Guillot, S., and Le Fort, P. (1995) Geochemical constraints on the bimodal origin of High
373 Himalayan leucogranites. Lithos, 35, 221-234.
374 Helms, T.S., and Labotka, T.C. (1991) Petrogenesis of Early Proterozoic pelitic schists of the
375 southern Black Hills, South Dakota: Constraints on regional low-pressure metamorphism.
376 Geological Society of America Bulletin, 103, 1324-1334.
377 Henry, D.J., and Guidotti, C.V. (1985) Tourmaline as a petrogenetic indicator mineral: an
378 example from the staurolite-grade metapelites of NW Maine. American Mineralogist, 70,
379 1-15.

Henry, D.J., and Dutrow, B.L. (1992) Tourmaline in a low grade clastic metasedimentary rock: an example of the petrogenetic potential of tourmaline. Contributions to Mineralogy and Petrology, 112, 203-218.

Henry, D.J., and Dutrow, B.L. (1996) Metamorphic tourmaline and its petrologic applications. Reviews in Mineralogy and Geochemistry, 33, 503-557.

Henry, D.J., Novak, M., Hawthorne, F.C., Ertl, A., Dutrow, B.L., Uher, P., and Pezzotta, F. (2011) Nomenclature of the tourmaline-supergroup minerals. American Mineralogist, 96, 895-913.

Huff, T.A., and Nabelek, P.I. (2007) Production of carbonic fluids during metamorphism of graphitic pelites in a collisional orogen - An assessment from fluid inclusions. Geochimica et Cosmochimica Acta, 71, 4997-5015.

Jolliff, B.L., Papike, J.J., Shearer, C.K., and Laul, J.C. (1986) Tourmaline as a recorder of pegmatite evolution: Bob Ingersoll pegmatite, Black Hills, South Dakota. American Mineralogist, 71, 472-500.

Keller, P., Robles, E.R., Perez, A.P., and Fontan, F. (1999) Chemistry, paragenesis and significance of tourmaline in pegmatites of the Southern Tin Belt, central Namibia. Chemical Geology, 158, 203-225.

Leeman, W.P., and Sisson, V.B. (1996) Geochemistry of boron and its implications for crustal and mantle processes. Reviews in Mineralogy and Geochemistry, 33, 645-707.

Maloney, J.S., Nabelek, P.I., Sirbescu, M.C., and Halama, R. (2008) Lithium and its isotopes in tourmaline as indicators of the crystallization process in the San Diego County pegmatites, California, USA. European Journal of Mineralogy, 20, 905-916.

403 Manning, C.E., Wilke, M., Schmidt, C., and Cauzid, J. (2008) Rutile solubility in albite-H_2O and
404 $Na_2Si_3O_7$-H2O at high temperatures and pressures by in-situ synchrotron radiation micro-
405 XRF. Earth and Planetary Science Letters, 272, 730-737.
406 Moran, E.A., Sisson, V.B., and Leeman, W.P. (1992) Boron depletion during progressive
407 metamorphism: Implications for subduction processes. Earth and Planetary Science
408 Letters, 111, 331-349.
409 Nabelek, P.I. (2019) Petrogenesis of leucogranites in collisional orogens. Geological Society,
410 London, Special Publications, SP491-2018.
411 Nabelek, P.I., and Bartlett, C.D. (1998) Petrologic and geochemical links between the post-
412 collisional Proterozoic Harney Peak leucogranite, South Dakota, USA, and its source
413 rocks. Lithos, 45, 71-85.
414 Nabelek, P.I., and Bartlett, C.D. (2000) Fertility of metapelites and metagraywackes during
415 leucogranite generation: an example from the Black Hills, U.S.A. Transaction of the
416 Royal Society of Edinburgh: Earth Sciences, 91, 1-14.
417 Nabelek, P.I., and Chen, Y. (2014) The initial garnet-in reaction involving siderite-rhodochrosite,
418 garnet re-equilibration and P-T-t paths of graphitic schists in the Black Hills orogen,
419 South Dakota, USA. Journal of Metamorphic Geology, 32, 133-150.
420 Nabelek, P.I., Denison, J.R., and Glascock, M.D. (1990) Behavior of boron during contact
421 metamorphism of calc-silicate rocks at Notch Peak, Utah. American Mineralogist, 75,
422 874-880.
423 Nabelek, P.I., Russ-Nabelek, C., and Denison, J.R. (1992a) The generation and crystallization
424 conditions of the Proterozoic Harney Peak leucogranite, Black Hills, South Dakota, USA:

Petrologic and geochemical constraints. Contributions to Mineralogy and Petrology, 110, 173-191.

Nabelek, P.I., Russ-Nabelek, C., and Haeussler, G.T. (1992b) Stable isotope evidence for the petrogenesis and fluid evolution in the Proterozoic Harney Peak leucogranite, Black Hills, South Dakota. Geochimica et Cosmochimica Acta, 56, 403-417.

Nabelek, P.I., Labotka, T.C., Helms, T.S., and Wilke, M. (2006) Fluid-mediated polymetamorphism related to Proterozoic collision of Archean Wyoming and Superior provinces in the Black Hills, South Dakota. American Mineralogist, 91, 1473-1487.

Norton, J.J., and Redden, J.A. (1990) Relations of zoned pegmatites to other pegmatites, granite, and metamorphic rocks in the southern Black Hills, South Dakota. American Mineralogist, 75, 631-655.

Ohmoto, H., and Kerrick, D. (1977) Devolatilization equilibria in graphitic systems. American Journal of Science, 277, 1013-1044.

Olivo, G.R., and Williams-Jones, A.E. (2002) Genesis of the auriferous C quartz-tourmaline vein of the Siscoe mine, Val d'Or district, Abitibi subprovince, Canada: structural, mineralogical and fluid inclusion constraints. Economic Geology, 97, 929-947.

Pichavant, M. (1981) An experimental study of the effect of boron on a water saturated haplogranite at 1 kbar vapour pressure. Contributions to Mineralogy and Petrology, 76, 430-439.

Redden, J.A., and DeWitt, E. (2008) Maps showing geology, structure, and geophysics of the central Black Hills, South Dakota. U.S. Geological Survey Scientific Investigations Map 2777, 44 pp.

Redden, J.A., Peterman, Z.E., Zartman, R.E., and DeWitt, E. (1990) U-Th-Pb geochronology and preliminary interpretation of the tectonic development of Precambrian rocks in the Black Hills. In J.F. Lewry and M.R. Stauffer, Eds., The Early Proterozoic Trans-Hudson Orogen, Geological Association of Canada Special Paper, 37, 229-251.

Rockhold, J.R., Nabelek, P.I., and Glascock, M.D. (1987) Origin of rhythmic layering in the Calamity Peak satellite pluton of the Harney Peak Granite, South Dakota: The role of boron. Geochimica et Cosmochimica Acta, 51, 487-496.

Shearer, C.K., Papike, J.J., Simon, S.B., Laul, J.C., and Christian, R.P. (1984) Pegmatite/wallrock interactions, Black Hills, South Dakota: Progressive boron metasomatism adjacent to the Tip Top pegmatite. Geochimica et Cosmochimica Acta, 48, 2563-2580.

Shearer, C.K., Papike, J.J., Simon, S.B., and Laul, J.C. (1986) Pegmatite-wallrock interactions, Black Hills, South Dakota: Interaction between pegmatite-derived fluids and quartz-mica schist wallrock. American Mineralogist, 71, 518-539.

Slack, J.F. (1996) Tourmaline associations with hydrothermal ore deposits. Reviews in Mineralogy and Geochemistry, 33, 559-643.

Teng, F., McDonough, W.F., Rudnick, R.L., and Walker, R.J. (2006) Diffusion-driven extreme lithium isotopic fractionation in country rocks of the Tin Mountain pegmatite. Earth and Planetary Science Letters, 243, 701-710.

von Goerne, G., and Franz, G. (2000) Synthesis of Ca-tourmaline in the system CaO-MgO-Al_2O_3-SiO_2-B_2O_3-H_2O-HCl. Mineralogy and Petrology, 69, 161-182.

468 von Goerne, G., Franz, G., and van Hinsberg, V.J. (2011) Experimental determination of Na-Ca
469 distribution between tourmaline and fluid in the system CaO-Na_2O-MgO-Al_2O_3-SiO_2-
470 B_2O_3-H_2O. The Canadian Mineralogist, 49, 137-152.
471 Wilke, M., Nabelek, P.I., and Glascock, M.D. (2002) B and Li in metapelites from the
472 Proterozoic Terrane in the Black Hills, South Dakota, USA: Implications for the origin of
473 leucogranitic magmas. American Mineralogist, 87, 491-500.
474

FIGURE CAPTIONS

Figure 1: Map showing the location of station 195 in the western aureole of the Harney Peak Granite (HPG). Thin solid lines are formation boundaries and thick solid lines are recognized faults. Thick dashed lines are isograds. Metamorphic zones are Grt = garnet, St = staurolite, Sil = sillimanite, and 2^{nd} Sil = second sillimanite where partial melting has occurred.

Figure 2: An image showing a quartz vein that is bounded by tourmalinite. A schist into which the tourmalinite grades is not shown in this image.

Figure 3: Thin-section images of **(a)** 195-1, **(b)** 195-3A, **(c)** 195-3B, and **(d)** 195-5. All images are in plain light and each field of view is 1 mm. **(a)** and **(c)** show tourmaline and graphite and some remnant anhedral quartz (white spots). **(b)** shows tourmaline within a 7 mm thick quartz vein cutting through 195-3B. **(d)** shows a biotite-muscovite schist with randomly-oriented tourmaline.

Figure 4: Back-scatter electron images of **(a)** sample 195-1 and **(b)** 195-3A. Each scale-bar represents 100 μm. Grey areas in tourmaline contain relatively low Fe/Al ratios. The ratio increases with brightness. Interstitial black patches are graphite. Quartz, also black, occurs as rounded inclusions in tourmaline.

Figure 5: (a) Relative occupancies of Al^{3+}, Fe^{2+}, and Mg^{2+} on tourmaline's Y sites in tourmalinite and HPG. Compositions of tourmaline in the HPG are given in Supplementary Material. **(b)** Average molar proportions of Al_2O_3, FeO, and MgO in individual grains of

498 tourmaline in samples 195-1, 195-3A, 195-3B, and 195-5, in biotite and muscovite in 195-5, and
499 in biotite in other Black Hills schists (Nabelek and Bartlett, 2000; compositions given in
500 Supplementary Material).
501
502 **Figure 6:** Variations of selected ions and X-site vacancies with $^{Y}Al^{3+}$ in metasomatic tourmaline.
503 Lines through data are linear regressions given in Table 2. Fe^{2+} contributes more than Mg^{2}+ to a
504 tight combined correlation of $^{Y}(Fe^{2+}+Mg^{2+})$ with $^{Y}Al^{3+}$. Na^{+} and O^{2-} do not show significant
505 correlations with $^{Y}Al^{3+}$.
506

TABLE 1. Compositions of tourmaline with minimum and maximum ^{Y}Al in each sample

	195-1 min. ^{Y}Al	195-1 max. ^{Y}Al	195-3A min. ^{Y}Al	195-3A max. ^{Y}Al	195-3B min. ^{Y}Al	195-3B max. ^{Y}Al	195-5 min. ^{Y}Al	195-5 max. ^{Y}Al
Oxides								
SiO_2	34.71	35.19	34.26	32.51	35.10	35.29	35.40	35.37
TiO_2	1.03	0.92	1.47	0.20	0.96	0.33	0.83	0.53
Al_2O_3	30.94	32.14	30.18	34.11	31.35	33.59	32.02	32.88
FeO	9.29	8.28	10.77	8.30	9.75	7.81	7.90	7.43
MnO	0.05	0.03	0.05	0.04	0.05	0.04	0.02	0.03
MgO	5.31	5.26	4.52	4.40	5.48	5.22	5.63	5.58
CaO	0.75	0.37	0.90	0.13	0.80	0.20	0.34	0.30
Na_2O	2.03	2.04	1.73	1.78	1.98	2.05	2.04	2.08
K_2O	0.02	0.01	0.03	0.01	0.03	0.01	0.01	0.02
F[c]	–	–	–	–	0.09	–	–	–
B_2O_3[b]	10.16	10.26	10.05	10.01	10.33	10.37	10.29	10.32
H_2O[b]	3.22	3.20	3.20	3.48	3.33	3.31	3.24	3.23
O=F	–	–	–	–	0.04	–	–	–
Total	97.50	97.71	97.17	94.97	99.23	98.23	97.72	97.77
Site occupancies								
B[a]	3.000	3.000	3.000	3.000	3.000	3.000	3.000	3.000
^{T}Si	5.939	5.961	5.925	5.645	5.906	5.917	5.982	5.956
^{T}Al	0.061	0.039	0.075	0.355	0.094	0.083	0.018	0.044
^{Z}Al	6.000	6.000	6.000	6.000	6.000	6.000	6.000	6.000
^{Y}Al	0.178	0.378	0.079	0.624	0.123	0.554	0.359	0.484
^{Y}Ti	0.132	0.117	0.191	0.026	0.122	0.042	0.105	0.067
^{Y}Fe	1.330	1.174	1.558	1.205	1.372	1.095	1.116	1.046
^{Y}Mn	0.007	0.005	0.008	0.006	0.008	0.006	0.003	0.004
^{Y}Mg	1.353	1.327	1.164	1.137	1.375	1.304	1.417	1.399
^{X}Ca	0.137	0.067	0.167	0.024	0.144	0.035	0.062	0.053
^{X}Na	0.672	0.670	0.581	0.599	0.647	0.667	0.669	0.680
^{X}K	0.004	0.002	0.007	0.002	0.006	0.003	0.001	0.005
^{X}vacancy	0.187	0.261	0.245	0.375	0.203	0.295	0.267	0.262
^{V}OH	3	3	3	3	3	3	3	3
^{W}OH	0.670	0.621	0.691	1.000	0.737	0.705	0.654	0.634
^{W}F[c]	–	–	–	–	0.048	–	–	–
^{W}O	0.330	0.379	0.309	0.000	0.215	0.295	0.346	0.366

[a] Assumed occupancy.

[b] Calculated by assuming 3 boron atoms and 15 Y+Z+T cations.

[c] Fluorine was analyzed in only a subset of samples (see Supplementary Materials).

TABLE 2. Regressions of element occupancies with ^{Y}Al

Element or vacancies	regression	R^2
Fe + Mg	$-0.77 \times {}^{Y}Al + 2.82$	0.92
Fe	$-0.65 \times {}^{Y}Al + 1.49$	0.55
Mg	$-0.12 \times {}^{Y}Al + 1.33$	0.04
Ti	$-0.24 \times {}^{Y}Al + 0.17$	0.74
Ca	$-0.31 \times {}^{Y}Al + 0.20$	0.87
Na	$-0.04 \times {}^{Y}Al + 0.66$	0.02
Vacancies X	$0.36 \times {}^{Y}Al + 0.13$	0.70

TABLE 3. Tourmaline compositions (apfu) used in computing substitution 3

Element	Tourmaline ($^{Y}Al = 0.0$)	Tourmaline ($^{Y}Al = 0.66$)
^{T}Si	6.00	6.00
^{T}Al	0.00	0.00
^{Z}Al	6.00	6.00
^{Y}Al	0.00	0.66
$^{Y}(Fe+Mg)$	2.82	2.34
^{Y}Ti	0.18	0.00
^{X}Ca	0.18	0.00
^{X}Na	0.64	0.67
$^{X}vacancy$	0.18	0.33
^{W}OH	0.64	0.67
^{W}O	0.36	0.33

TABLE 4. Mineral compositions (apfu) used in reactions 5 and 6

Element	Tourmaline (^{Y}Al = 0.1)	Tourmaline (^{Y}Al = 0.66)	Biotite	Muscovite
Si	5.922[a]	5.922[a]	2.688	3.054
Ti	0.146	0	0.105	0.015
Al	6.178	6.738	1.737	2.831
Fe	1.425	1.061	1.466	0.071
Mg	1.318	1.251	0.865	0.046
Ca	0.169	0	0	0
Na	0.650[a]	0.650[a]	0.039	0.187
K	0	0	0.877	0.809
B	3.000	3.000	0.000	0.000
H	3.660[a]	3.660[a]	2.000	2.000
O	31.000	31.000	12.000	12.000

[a] Because there is no significant correlation of these cations with ^{Y}Al in tourmaline, average concentrations were used to calculate reactions.

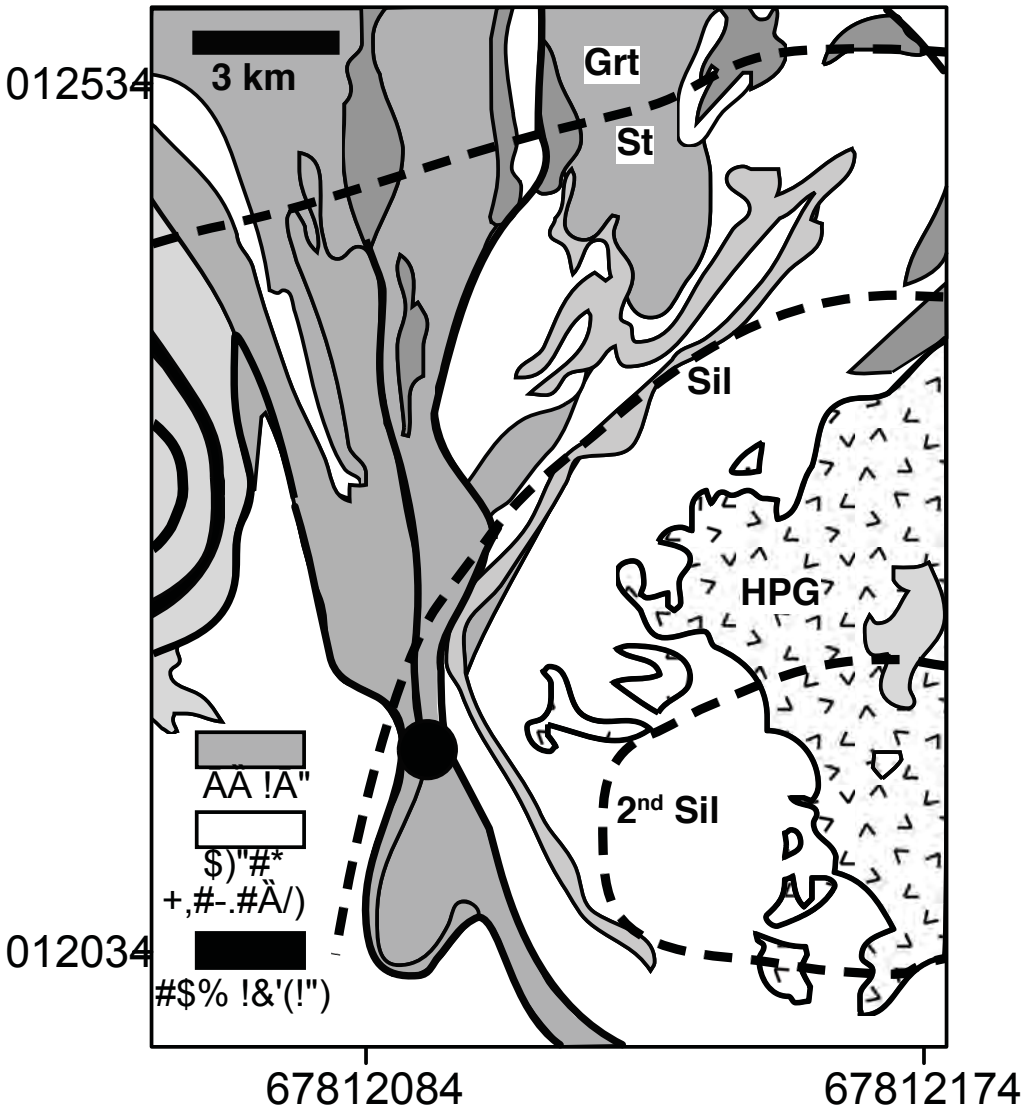
012534
012034
3 km
Grt
St
Sil
HPG
2nd Sil
AÀ !A"
$)"#*
+,#-.#À/)
#$% !&'(!")
67812084
67812174

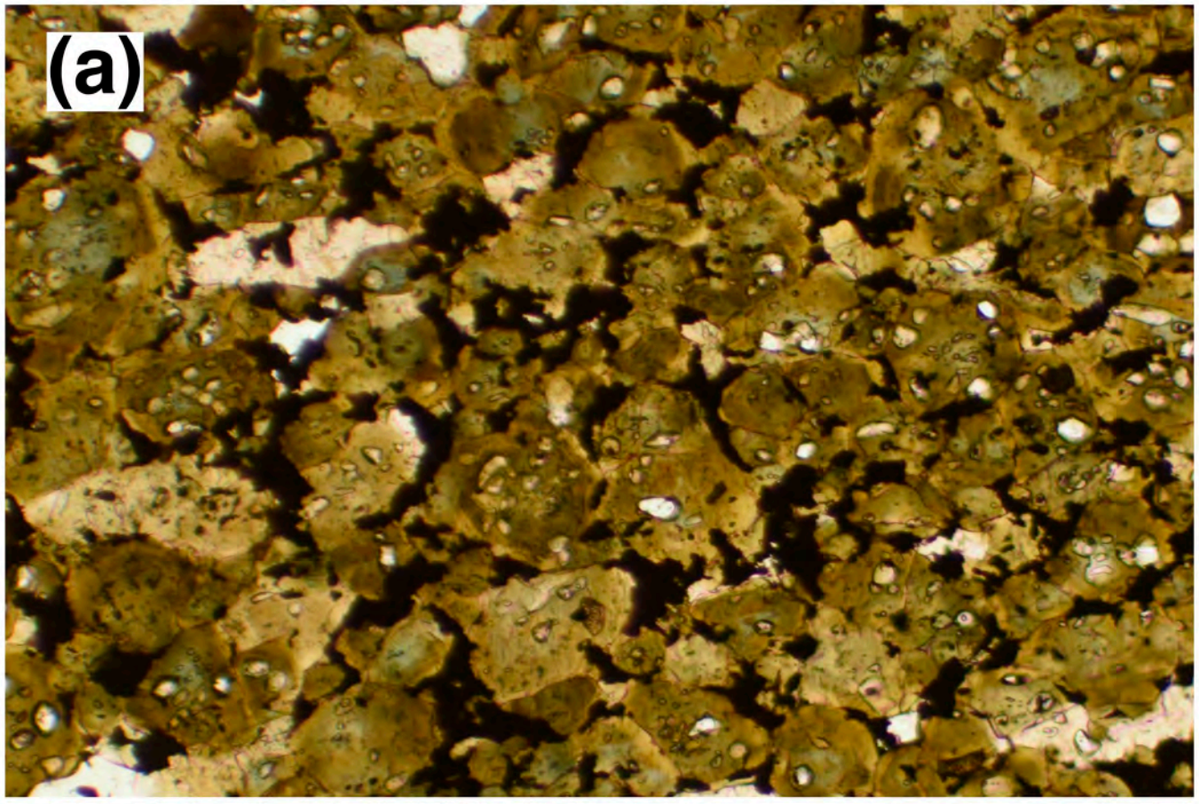
(a)

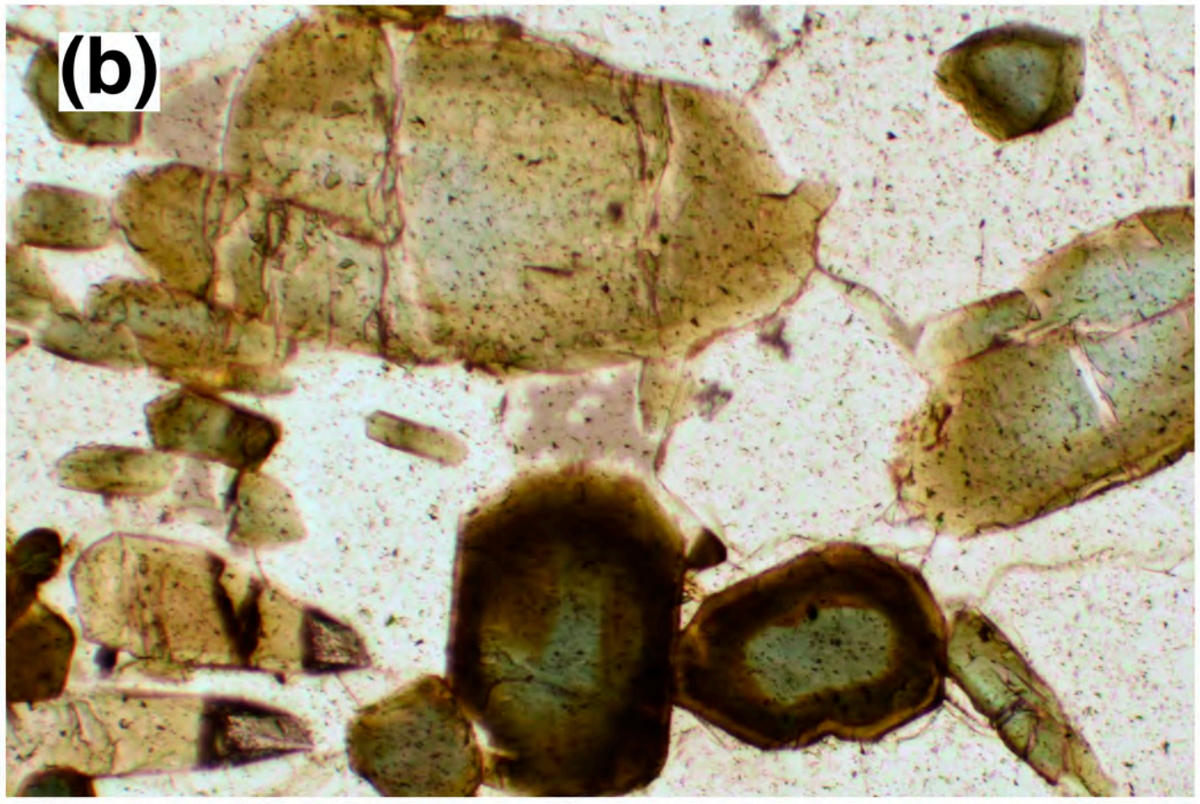
(b)

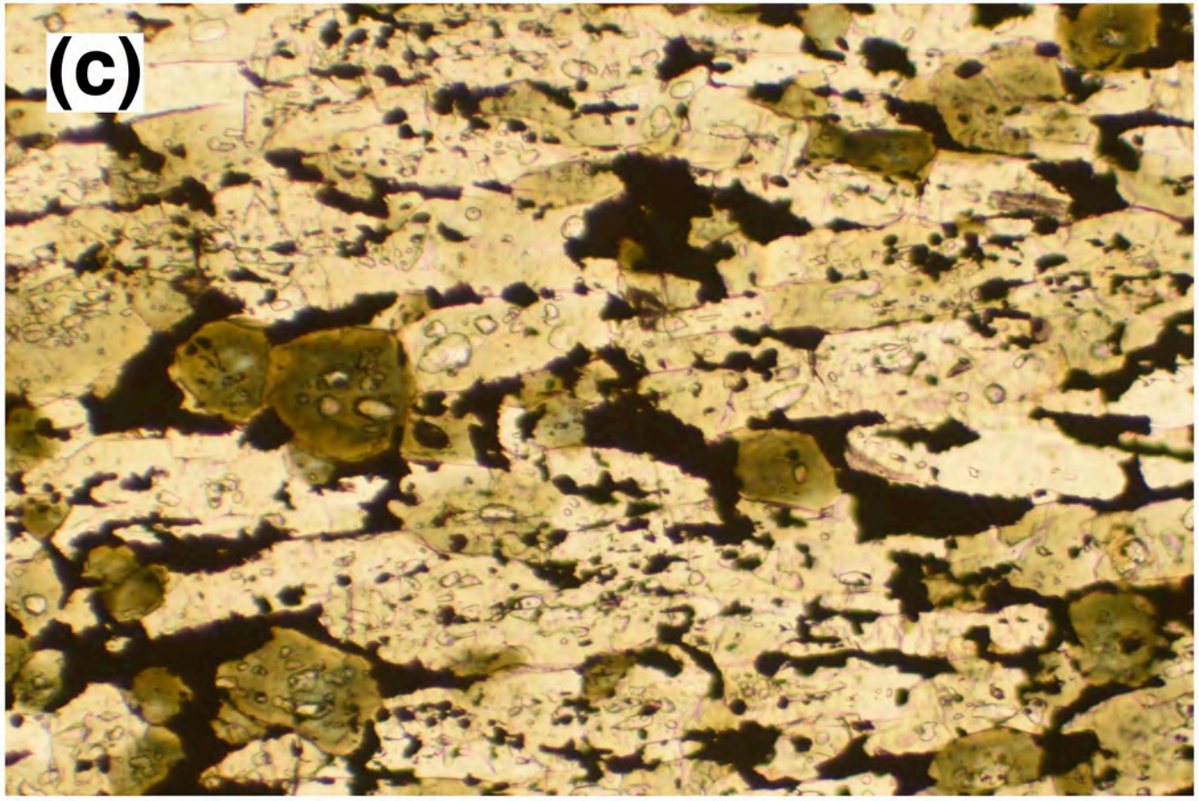
(c)

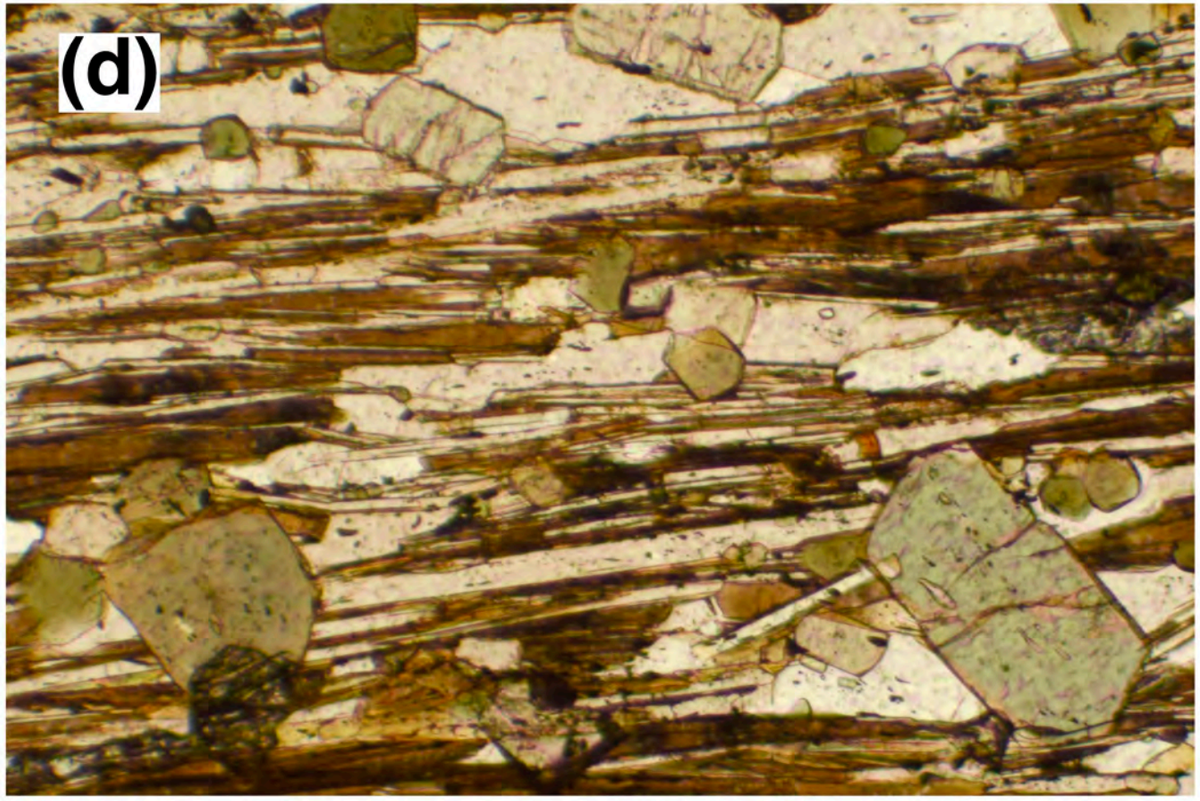
(d)

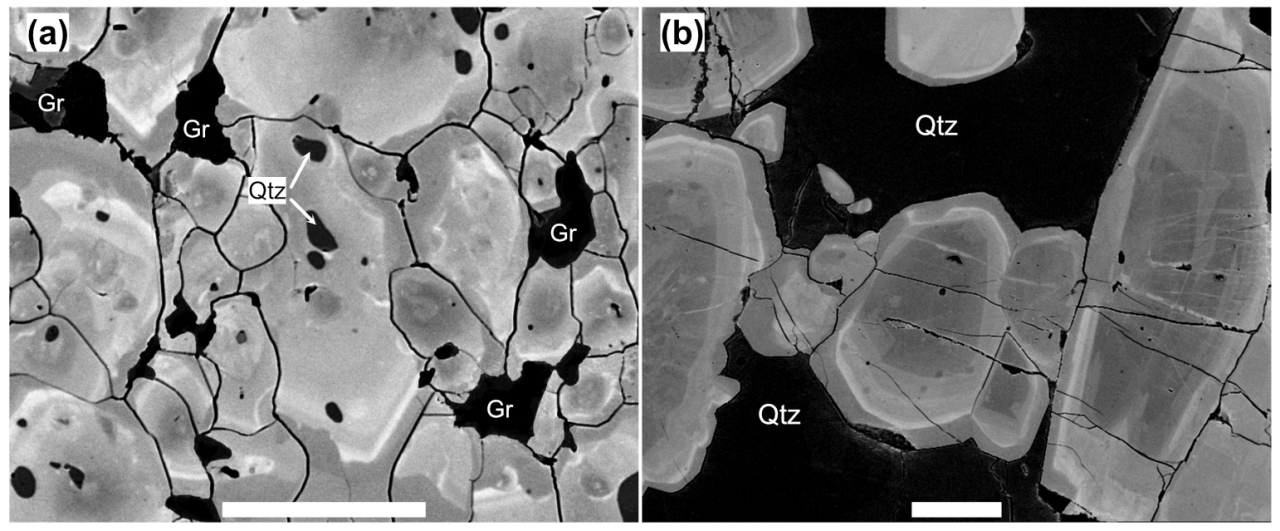
(a)
Gr
Gr
Qtz
Gr
Gr
(b)
Qtz
Qtz

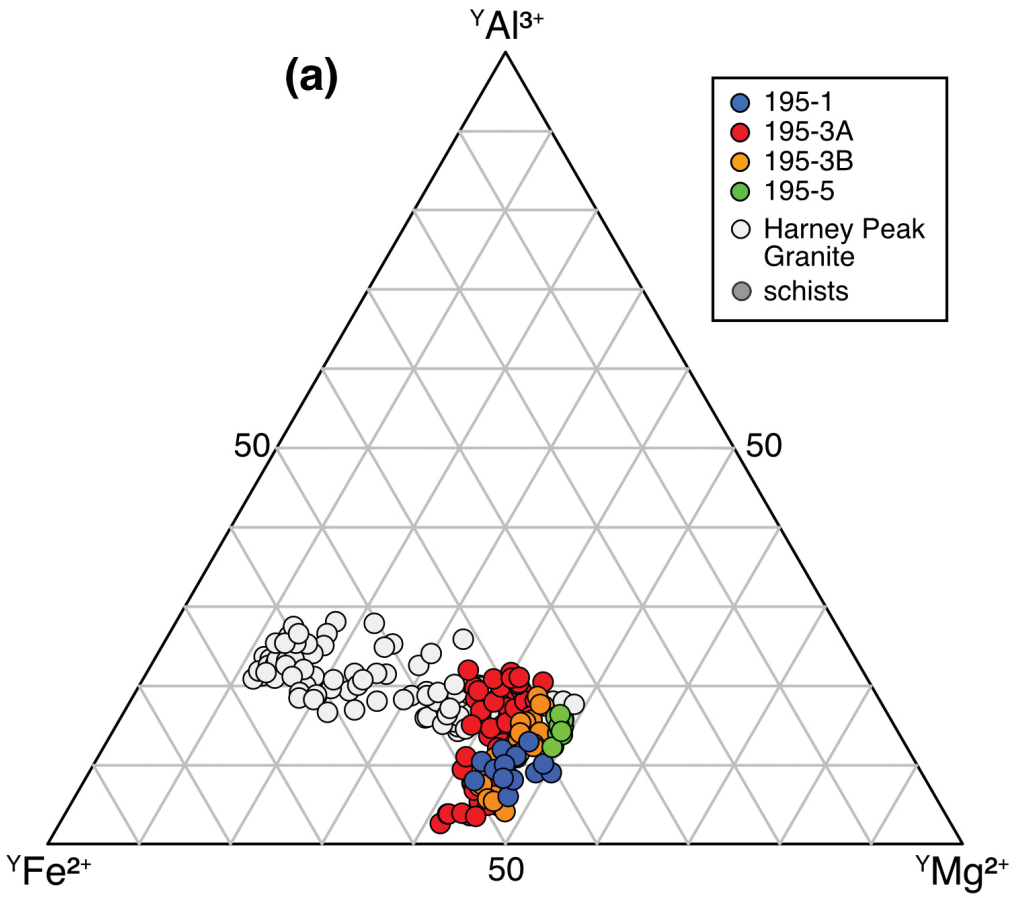
(a)
$^{Y}Al^{3+}$
195-1
195-3A
195-3B
195-5
Harney Peak Granite
schists
50
50
$^{Y}Fe^{2+}$
50
$^{Y}Mg^{2+}$

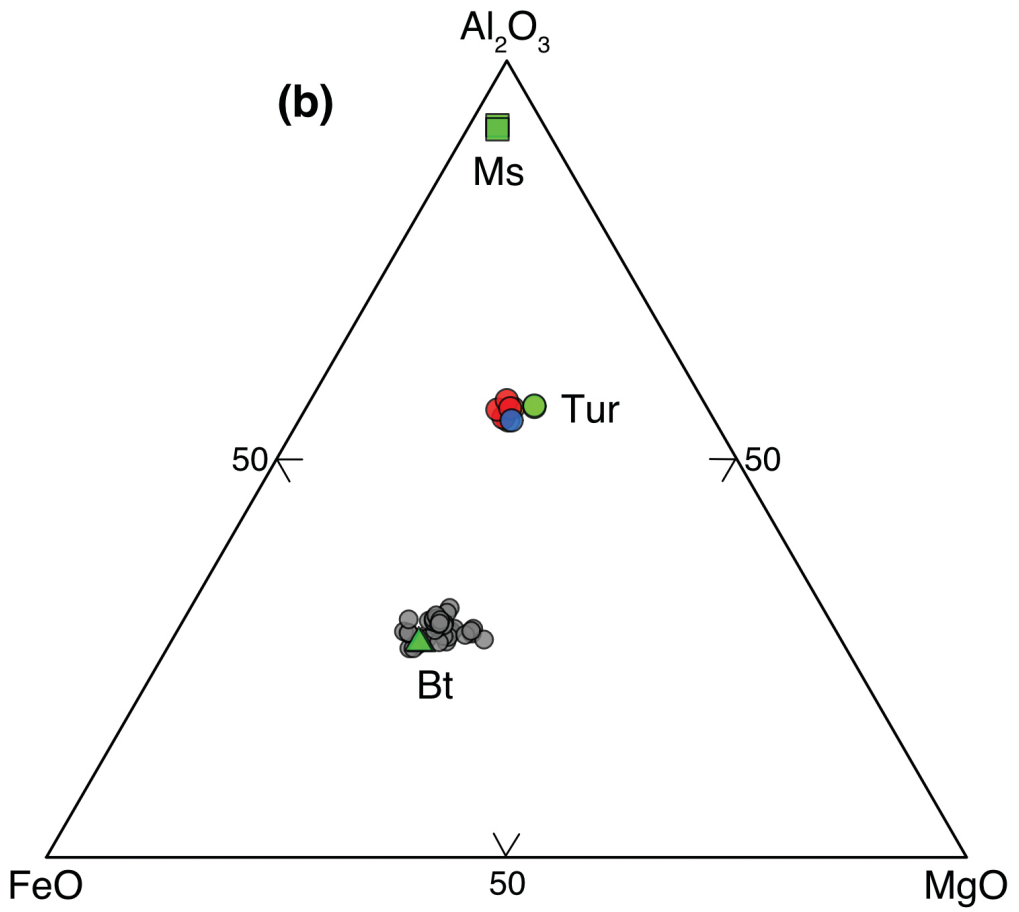
(b)
Al_2O_3
Ms
Tur
Bt
50
50
FeO
50
MgO

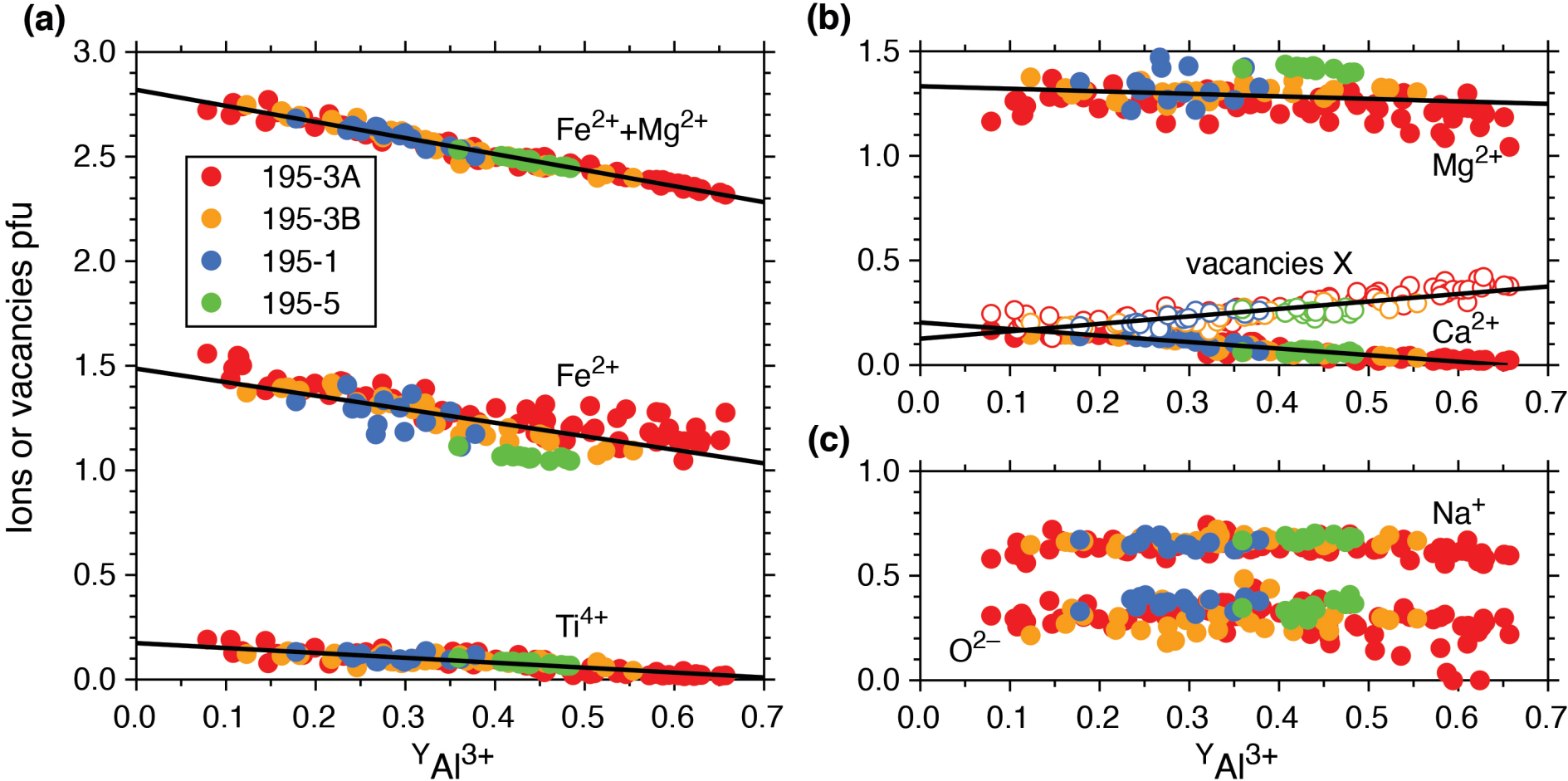
(a)
(b)
(c)
Ions or vacancies pfu
$^{Y}Al^{3+}$
$Fe^{2+}+Mg^{2+}$
Fe^{2+}
Ti^{4+}
195-3A
195-3B
195-1
195-5
Mg^{2+}
vacancies X
Ca^{2+}
Na^{+}
O^{2-}